*Acta Oceanol. Sin.*, 2017, Vol. 36, No. 5, P. 83–89
DOI: 10.1007/s13131-017-1062-7
http://www.hyxb.org.cn
E-mail: hyxbe@263.net

# An advanced wind vector retrieval algorithm for the rotating fan-beam scatterometer

XIE Xuetong[1]*, WEN Ya[2], HUANG Zhou[3]

[1] School of Geographical Sciences, Guangzhou University, Guangzhou 510006, China

[2] College of Natural Resources and Environment, South China Agricultural University, Guangzhou 510642, China

[3] Institue of Remote Sensing and Geographical Information System, Peking University, Beijing 100871, China

Received 7 May 2016; accepted 29 July 2016



**Abstract**

The rotating fan-beam scatterometer (RFSCAT) is a new type of satellite scatterometer that is proposed approximately 10 a ago. However, similar to other rotating scatterometers, relatively larger wind retrieval errors occur in the nadir and outer regions compared with the middle regions of the swath. For the RFSCAT with the given parameters, a wind direction retrieval accuracy decreases by approximately 9 in the outer regions compared with the middle region. To address this problem, an advanced wind vector retrieval algorithm for the RFSCAT is presented. The new algorithm features an adaptive extension of the range of wind direction for each wind vector cell position across the whole swath according to the distribution histogram of a retrieved wind direction bias. One hundred orbits of Level 2A data are simulated to validate and evaluate the new algorithm. Retrieval experiments demonstrate that the new advanced algorithm can effectively improve the wind direction retrieval accuracy in the nadir and outer regions of the RFSCAT swath. Approximately 1.6 and 9 improvements in the wind direction retrieval are achieved for the wind vector cells located at the nadir and the edge point of the swath, respectively.

**Key words:** rotating fan-beam scatterometer, objective function, wind vector retrieval, distribution histogram of bias, wind direction extension

**Citation:** Xie Xuetong, Wen Ya, Huang Zhou. 2017. An advanced wind vector retrieval algorithm for the rotating fan-beam scatterometer. Acta Oceanologica Sinica, 36(5): 83–89, doi: 10.1007/s13131-017-1062-7

## 1 Introduction

The concept of the rotating fan-beam scatterometer (RFSCAT) was first introduced approximately 10 a ago (Lin et al., 2003; Kloe and Stoffelen, 2003). The RFSCAT assimilates advantages of both fan-beam and rotating scatterometers. Simulation experiments indicate that it can achieve a higher wind vector retrieval accuracy than other traditional scatterometers, such as SeaWinds, ASCAT, and HY-2 SCAT. The relatively higher performance of the RFSCAT comes from the diversity of its incidence and azimuth angles. However, similar to other rotating scatterometers (SeaWinds and HY-2), the wind vector retrieval accuracy of the RFSCAT varies with the wind vector cell position of the swath. The wind retrieval errors in the nadir and outer regions are relatively larger than those in the middle regions. For the RFSCAT with the parameters given in this paper, the wind direction retrieval accuracy decreases by approximately 9° in the outer regions compared with that in the nadir region. Thus, it is necessary to establish an appropriate algorithm that can make full use of the incidence and azimuth diversities to further enhance the wind retrieval accuracy of the RFSCAT, especially in the nadir and outer regions. Although wind retrieval algorithms for traditional scatterometers (SeaWinds, NSCAT, ASCAT, and HY-2 SCAT) have been extensively investigated, an effective algorithm for the RFSCAT has been less studied in the past decade (Arnús, 2002; Xie et al., 2013; Wang et al., 2015).

According to the characteristics of the RFSCAT, we developed an end-to-end simulation software for this type of scatterometer. The RFSCAT alternately transmits HH and VV microwave pulses to the ocean surface when the antenna rotates around its axis. Simulation experiments indicate that the distribution of the objective function near the local maxima is flatter in the nadir and outer regions than in the middle region of the swath. On the basis of this feature of the objective function, an advanced wind vector retrieval algorithm for the RFSCAT was derived in this paper. Retrieval experiments were conducted using the simulated backscatter coefficient data generated by the simulation software. The experiment results demonstrate that the newly established algorithm can effectively improve the wind direction retrieval accuracy in the nadir and outer regions of the RFSCAT swath.

The rest of this paper is organized as follows. Section 2 gives a detailed description of the advanced algorithm derived in this paper. Simulation methods and parameters are briefly presented in Section 3. In Section 4, the experiment results are analyzed and discussed. Finally, conclusions are drawn in Section 5.

## 2 The advanced algorithm

Among the existing algorithms, a Maximum Likelihood Es-

Foundation item: The National Natural Science Foundation of China under contract Nos 41476152 and 41506206; the National High Technology Research and Development Program (863 Program) of China under contract No. 2013AA09A505; the Major Project on the Integration of Industry, Education, and Research of Guangzhou City of China under contract No. 201508020109.
*Corresponding author, E-mail: xtxie2013@163.com

timation (MLE) algorithm is assumed to be the best for the scatterometer wind vector retrieval due to the high retrieval precision and complete independence of the model function (Freilich, 2000; Chi and Li, 1988). However, for the rotating scatterometer, wind retrieval errors are larger in the nadir and outer regions of the swath because of its inherent observing geometry. To improve the retrieval accuracy in the nadir region, Stiles et al. (2002) proposed a direction interval retrieval (DIR) algorithm for the SeaWinds scatterometer. However, simulation experiments indicate that this type of wind direction ambiguity exists not only in the nadir region but also in the outer and middle regions of the swath. On the basis of the main idea of the DIR algorithm proposed by Stiles et al. (2002), we modified the traditional MLE algorithm by extending the range of the wind direction for the whole swath.

### 2.1 *MLE objective function*

An MLE objective function (Freilich, 2000) is used for the RFSCAT wind retrieval because of its advantages mentioned above. It can be written as follows:

$$J_{MLE}(w,\Phi)=-\sum_{i=1}^{N}\left\{\frac{[z_i-M(w,\Phi-\varphi_i,\theta_i,p_i)]^2}{V_{ri}}+\ln V_{ri}\right\}, \quad (1)$$

where $z$ and $M$ represent the measured backscatter coefficient and the model value, respectively; $V_r$ is the measurement variance; and $w$, $\Phi$, $\varphi$, $\theta$, and $p$ denote the wind speed, the wind direction, the radar azimuth, the incidence angle, and the polarization, respectively. The purpose of the wind retrieval is to find the appropriate wind vectors that maximize Eq. (1).

### 2.2 *Modified wind vector retrieval algorithm*

A wind direction extension is an important part of the algorithm design. The change rate of the objective function along the wind direction is adopted as the criterion for the wind direction extension and is defined as follows:

$$k=\frac{|J_r-J_l|}{2\Delta d}, \quad (2)$$

where $J_r$ and $J_l$ are the local maximum objective function values at neighboring right and left wind directions, respectively; and $\triangle d$ is the wind direction interval.

The wind direction extension algorithm consists of two procedures, namely, left-extension and right-extension. The left-extension algorithm contains the following steps.

(1) Take the wind direction of the ambiguity solution as the right wind direction $d_r$ and calculate the current wind direction $d_c$ using the following equation:

$$d_c=d_r-\Delta d=\begin{cases}d_c & \text{if} \quad d_c\geqslant 0\\ d_c+360^\circ & \text{else.}\end{cases}, \quad (3)$$

(2) Determine the maximum value of the objective function $J_c$ at the current wind direction using Eq. (1).

(3) Similarly, calculate the left wind direction $d_l$ using the following equation:

$$d_l=d_c-\Delta d=\begin{cases}d_l & \text{if} \quad d_l\geqslant 0\\ d_l+360^\circ & \text{else.}\end{cases}, \quad (4)$$

(4) Determine the maximum value of the objective function $J_l$ at the left wind direction.

(5) Calculate the change rate of the objective function with the wind direction using Eq. (2).

(6) Update the right and current direction with the current and left direction, and repeat Steps (2) to (6) until the change rate $k$ is larger than the given threshold $k_0$.

Thus, the last current wind direction is the left-extension boundary when the iterative process stops. The right-extension has similar processing steps.

It is difficult to determine a rate threshold that is appropriate for all regions of the RFSCAT swath. Experiments show that the best method is to set a different rate threshold for each wind vector cell position across the swath. In this paper, we determined the rate threshold value according to the distribution histogram of the bias between the retrieved wind direction and the "real" wind direction. Only the first and second ambiguity wind directions were considered in the histogram analysis.

Here, the wind direction bias refers to the difference between the retrieved wind direction and the reference, or "real", wind direction. The retrieved wind directions were obtained by using the traditional MLE wind vector retrieval algorithm. There is a tight relationship between the change rate of the objective function and the width of the bias distribution.

The wind direction extension values are the wind direction boundary values after the wind direction range extension, which is an important part of the modified algorithm. Therefore, the extent of similarity between these two histograms can reflect if the change rate threshold values are suitably set or not. Simulation experiments indicated that the rate threshold in the middle region should be larger than that in the nadir and outer regions of the swath in order to achieve good retrieval performance.

The proportion of the wind vector cells with a certain wind direction bias can be defined as follows:

$$P(b)=\frac{N_b}{N}, \quad (5)$$

where $N_b$ is the number of wind vector cells that have the wind direction bias $b$; and $N$ is the total wind vector cells in the statistical analysis. The wind direction bias is calculated by the following formula:

$$b=d_m-d_0, \quad (6)$$

where $d_m$ and $d_0$ represent the retrieved wind direction and the true wind direction, respectively. Note that the wind direction bias $b$ should be transformed into the range of [–180°, 180°] as follows:

$$b=\begin{cases}b & \text{if} \quad 0^\circ\leqslant b\leqslant 180^\circ \text{or} -180^\circ\leqslant b<0^\circ,\\ b-360^\circ & \text{if} \quad 180^\circ<b<360^\circ,\\ b+360^\circ & \text{if} \quad -360^\circ<b<-180^\circ.\end{cases} \quad (7)$$

Similarly, the proportion of the wind vector cells with a certain wind direction extension boundary value $d$ can be calculated by

$$P(d)=\frac{N_d}{N}, \quad (8)$$

where $N_d$ is the number of the wind vector cells associated with

the wind direction ($d$) extension value, which is the last current wind direction $d_c$ after extension.

As discussed above, the proportion of the wind vector cells depends on and is sensitive to the rate threshold $k_0$ value. The larger rate threshold is, the larger wind direction extension is, and the wider the distribution histogram of the wind direction extension value becomes. In theory, the similarity between the two histograms of the wind direction bias and the wind direction extension value should be high in order to obtain high wind retrieval performance. Therefore, it is a key step to adjust the given threshold to make the two histograms more similar in the advanced algorithm design.

The threshold values of the change rate of the objective function for each wind vector cell column used in this paper are shown in Fig. 1. From Fig. 1, it can be seen that the curve of the threshold value shows an M shape, which is opposite to the shape of the wind retrieval error curve. This indicates that larger change rates are required to obtain a wide enough range of the wind direction in the middle regions of the swath.

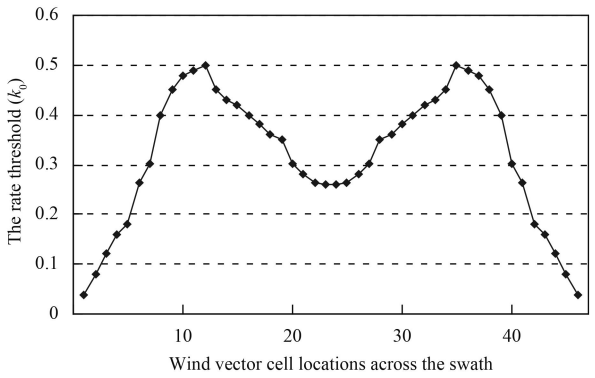


**Fig. 1.** The curve of the threshold value versus the wind vector cell location across the swath.

Figures 2 and 3 give the distribution histograms of the wind direction bias and the corresponding wind direction extension values respectively. In the simulation experiments, the NCEP wind direction from the SeaWinds L2B data file is taken as the reference wind direction, which is one of the data input into the simulation software.

Owing to limited space, only three histograms for typical locations in the RFSCAT swath (Columns 1, 12, and 23) are given in Figs 2 and 3. In our simulation software, the size of the wind vector cell is set to 25 km, and there are 46 wind vector cells in one row. Thus, Columns 1, 12, and 23 are located in the outer, middle, and nadir regions, respectively. Figures 2 and 3 indicate that the histograms for the wind direction bias and the wind direction extension are very similar in terms of distribution characteristics. In both cases, the distribution width first decreases and then increases when the column number varies from 1 to 23. The distribution width peaks at Columns 1 and 46, implying the greatest uncertainty in the wind direction retrieval for these locations.

### 2.3 *Modified circle median filter algorithm*

In addition, modifications should also be made to a circle median filter algorithm in order to let it select more possible wind directions in the process of the ambiguity removal.

According to the distribution characteristics of the histograms, the swath can be divided into three regions in the ambiguity removal (Xie et al., 2010). The swaths of the RFSCAT are partitioned as follows:

(1) In the nadir region: Columns 16 to 31;

(2) In the middle region: Columns 7 to 15 and 32 to 40;

(3) In the outer region: Columns 1 to 6 and 41 to 46.

The concept of a circle median filter was first extended and applied to wind vector data by Shaffer et al. (1991). According to Shaffer et al.(1991), the definition of a circle median can be written as follows:

$$A^* = \min_k \sum_{m=i-h}^{i+h} \sum_{n=j-h}^{j+h} W_{mn} \left\| A_{ij}^k - A_{mn} \right\|, \tag{9}$$

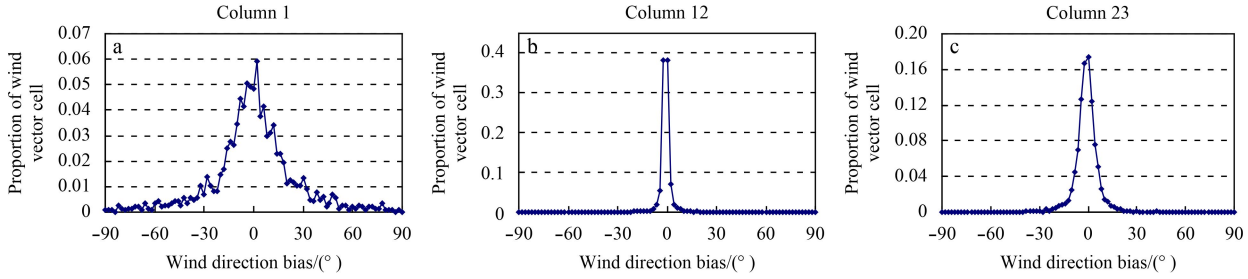


**Fig. 2.** The distribution histograms of the wind direction bias for different wvc columns.

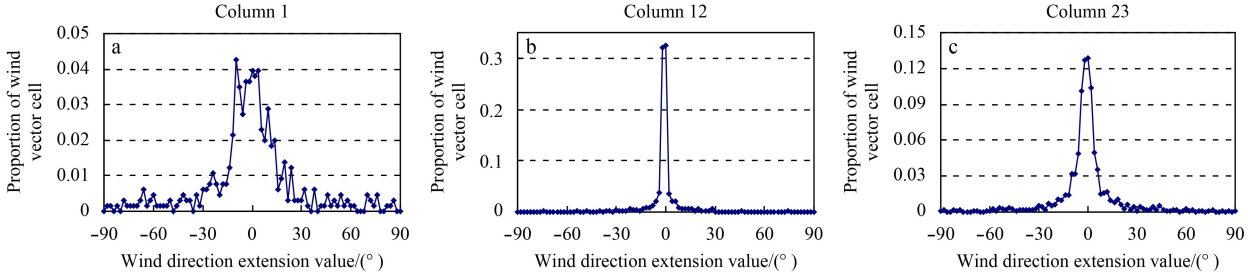


**Fig. 3.** The distribution histograms of the wind direction extension for different wvc columns.

where $(i, j)$ is the center of the filter window with size $N$ ($N$ is an odd number); $h$=($N$–1)/2; $A_{ij}^{k}$ denotes the $k$th wind vector ambiguity solution of the window center; $A_{mn}$ is the current ambiguity solution located at position $(m, n)$ in the filter window; and $W_{mn}$ is the corresponding weight coefficient at the same position.

The modified circle median filter algorithm for an ambiguity removal is composed of three steps.

(1) Initialize the wind field using the first ambiguities and apply the circle median filter along the column direction in the middle regions.

(2) Take the filtered wind field from Step (1) as a reference, and apply the extending filter from the boundaries of the middle regions to the nadir and outer regions. The moving direction of the filter window is also along the column.

(3) On the basis of the filtered results from Steps (1) and (2), apply the circle median filter to the entire swath along the row direction.

It is noted that the filter algorithm should also be improved to make it consider more possible wind directions when determining the circle median in Steps (1) and (2). The traditional circle median filter algorithm is adopted in Step (3) to prevent it from not converging.

The procedures of the improved filter algorithm are as follows.

(1) Construct the extended wind direction array using the boundary values after extension and the wind direction interval to save the possible wind direction set. Assume there are four ambiguities in the current wind vector cell, with the wind directions represented by $d_1$, $d_2$, $d_3$, and $d_4$. Then, the extended wind direction ranges of the first and second ambiguities can be denoted as below:

$$D_1 = [d_{1l}, d_{1r}], \tag{10a}$$

$$D_2 = [d_{2l}, d_{2r}], \tag{10b}$$

where $d_{1l}$ and $d_{1r}$ are the left boundary and right boundary values of the first ambiguity after extension; and $d_{2l}$ and $d_{2r}$ are the corresponding values of the second ambiguity. The whole set of possible wind directions to be used in the ambiguity removal can be expressed as

$$D = \{D_1, D_2, d_3, d_4\}. \tag{11}$$

(2) Determine the circle median of the window center using Eq. (9), and record its array index.

(3) Determine which ambiguity the circle belongs to based on its array index.

(4) If the circle median wind direction lies in the extended wind direction of the first ambiguity or the extended wind direction of the second ambiguity, then search for the wind speed that maximizes Eq. (1) for the current wind direction. The calculated wind speed and the circle median wind direction compose the circle median ambiguity. If the circle median wind direction is equal to the third ambiguity or the fourth ambiguity, then the third or fourth ambiguity is the circle median ambiguity.

(5) Replace the current ambiguity at the window center with the circle median ambiguity.

## 3 Simulation method and parameters

Because of the lack of real measurement data, an end-to-end simulation software for the RFSCAT was developed to provide the simulated backscatter data and to validate the new algorithm. The simulation software developed in this paper includes six functional modules, as shown in Fig. 4.

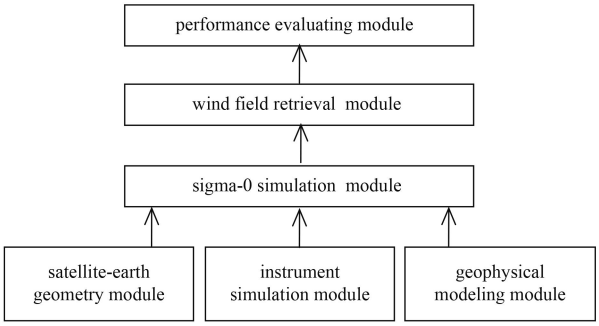


**Fig. 4.** The functional modules of the simulation software for the RFSCAT.

The radar equation is the basic theory for the wind vector retrieval from the microwave scatterometers. According to the radar equation, the received power by a scatterometer (Ulaby et al., 1986) can be calculated as follows:

$$P_r = \frac{P_t \lambda^2}{(4\pi)^3 L_f} \iint_{\Omega} \frac{G_t G_r \sigma^0}{R^4} \mathrm{d}A, \tag{12}$$

where $P_t$ and $P_r$ are the transmit and backscattered powers, respectively; $\lambda$ is the radar wavelength; $L_f$ denotes the system losses; $\Omega$ represents the area illuminated by the radar beam; $\sigma^0$ is the backscatter coefficient of the ocean surface; $R$ is the slant range; and $G_t$ and $G_r$ are the transmit and receive one-way gains of the radar antenna.

When the instrument noise is taken into account in the modeling, the relationship between the backscatter coefficient measurement and the actual received power can be written as

$$\hat{\sigma}^0 = \frac{\hat{P}_r}{X}, \tag{13}$$

where the symbol "^" denotes the corresponding measurement value including additional noise; and $X$ is the radar calibration factor as shown below:

$$X = \left[\frac{P_t \lambda^2}{(4\pi)^3 L_f}\right]^{-1} \left[\iint_{\Omega} \frac{G_t G_r}{R^4} \mathrm{d}A\right]^{-1}. \tag{14}$$

The quality of the retrieved wind vector field strongly depends on the level of the instrument noise. The parameter $K_p$ is commonly used as an indicator of the accuracy of a scatterometer measurement. It is defined as the normalized standard deviation of the measured backscatter power $\hat{P}_r$ or the measured backscatter coefficient $\hat{\sigma}^0$ (Long et al., 1988):

$$K_p = \frac{\sqrt{\delta^2\left(\hat{P}_r\right)}}{E\left(\hat{P}_r\right)} = \frac{\sqrt{\delta^2\left(\hat{\sigma}^0\right)}}{E\left(\hat{\sigma}^0\right)}, \tag{15}$$

where $\delta^2$ and $E$ denote calculating the variance and the mean value of a variable, respectively. The equation of the parameter $K_p$ for a Doppler scatterometer (Fischer, 1972) is

$$K_p = \sqrt{\frac{1}{T_p B_s}\left(1+\frac{1}{r_{sn}}\right)^2}, \tag{16}$$

where $r_{sn}$ is the signal-to-noise ratio; $T_p$ and $B_s$ are the time length of the radar pulses and the Doppler bandwidth of the echo signals associated with each slice. The product of the time length of the radar pulses and the Doppler bandwidth of the echo signals determines the independent observation times of the radar pulses, which, in turn, influences the value of the parameter $K_p$ and thus the wind retrieval accuracy.

According to the definition of the parameter $K_p$, a smaller parameter is helpful for obtaining a higher accuracy of the wind retrieval. In Eq. (16), there is an inverse non linear relationship between the parameter $K_p$ and the SNR. Therefore, the larger the value of the SNR is, the smaller the value of the parameter $K_p$ and thus the higher the accuracy of the wind retrieval. In the design of a scatterometer, we always try to obtain a larger SNR in order to achieve higher wind retrieval performance.

Under the assumption that the measurement noise of the backscatter coefficient of the ocean surface is a Gaussian random variable, the measured backscatter coefficient can be simulated by the following equation:

$$\hat{\sigma}^0 = \sigma_m^0 + \sigma_m^0 K_p N(0,1), \tag{17}$$

where $\sigma_m^0$ represents the model value of the backscatter coefficient; and $N(0, 1)$ denotes a Gaussian distributed number with zero mean and unit variance, which is randomly generated.

Table 1 lists the key parameters of the RFSCAT simulation system.

**Table 1.** Key parameters for RFSCAT simulation

| Parameter | Value |
|---|---|
| Transmitted power/W | 129 |
| Antenna gain/dB | 30 (far end) |
| Radar wavelength/cm | 2.26 |
| Pulse width/ms | 3.5 |
| Pulse repeat time/ms | 17.6 for HH or VV |
| System loss/dB | 3 |
| Receive bandwidth/MHz | 1.5 |
| Noise factor/dB | 5 |
| Polarization | HH, VV (alternately) |
| Antenna rotation rate/r·min$^{-1}$ | 3.75 |
| Orbit height/km | 500 |
| Incidence angle/(°) | 28–51 |
| Footprint length/km | 300 |
| Footprint width/km | 12–17 |
| Wind vector cell/km×km | 25×25 |

It is noted that the pulse repeat time (PRT) is set to 17.6 ms, with 8.8 ms for each polarization (HH and VV). The two different polarization pulses are alternately transmitted and received by the radar antenna. The time length of 8.8 ms is sufficient for one pulse to be transmitted and received for the whole range of incidence angle (28°–51°). At an orbit altitude of 500 km, the slant range $R$ and the round-trip time are approximately 559 km and 3.8 ms for the near-end of the radar beam (28° incidence angle) and 755 km and 5.2 ms for the far-end (51° incidence angle), respectively. For a Doppler scatterometer, the sampling numbers $N_s$ of each echo signal can be defined as the product of the time length of the radar pulses and the Doppler bandwidth of the echo signals, and has no direct relationship with the PRT.

## 4 Retrieval experiments

### 4.1 *Data and parameters*

To avoid the effects of the random factors from some specific orbit data on the retrieval results, the new algorithm was validated by using 100 orbits of simulated RFSCAT L2A data and the collocated NCEP wind field data contained in the SeaWinds L2B file. Here, the NCEP wind data are referred to as the numerical weather prediction (NWP) wind products, which are routinely generated by a global forecast system (GFS) developed and maintained by the National Center for Environment Prediction (NCEP) (http://www.ncdc.noaa.gov/data-access/model-data/model-datasets/global-forcast-system-gfs). These wind data are also called GFS winds. The NCEP wind product has a spatial resolution of 0.5°×0.5° and needs to be temporally and spatially interpolated into the 25 km×25 km wind vector cell grids for collocation. Because the SeaWinds L2B files contain the quality collocated NCEP winds with a swath-based spatial framework, it is convenient for us to use these NCEP winds as the input wind fields for the RFSCAT data simulation. The SeaWinds L2B data can be obtained via the PO.DAAC FTP site: ftp://podaac.jpl.nasa.gov,in the pub/ocean_wind/seawinds/L2/directory (Lungu, 2001; Dunbar, 2006; JPL, 2003). Compared with the SeaWinds L2B winds, the wind directions of the NCEP have a better spatial consistency. However, the derived SeaWinds L2B winds have more errors and noise in their wind directions, which will influence the simulation effect. Therefore, the NCEP data were used as the input for the "real" wind field in this paper. The orbit numbers of the L2B data files used for the simulation are from 10 163 to 10 262. The maximum iteration times and window size for the circle median filter are 100 and 7×7, respectively.

The simulation software uses the input "reference" wind field data and instrument parameters of the RFSCAT to produce the simulated noisy backscatter measurement data. Then, the modified algorithm is run to perform the wind vector retrieval with the simulated backscatter coefficients.

### 4.2 *Results and analysis*

The wind vectors (speed and direction), mean absolute errors (MAEs), and root mean square errors (RMSEs) of the two algorithms for three different regions of the swath are calculated and given in Table 2. Table 2 shows that the modified algorithm can effectively improve the wind direction retrieval accuracy in the nadir and outer regions of the swath.

Figures 5 and 6 illustrate the variation curves of the wind speed and wind direction MAEs versus the wind vector cell location across the swath. Figure 4 clearly shows that the wind direction errors of the modified algorithm are lower than those of the traditional algorithm in the nadir and outer regions. Approximately 1.6° and 9° improvements in the wind direction retrieval accuracy are achieved for the wind vector cell nearest to (Column 23 or 24) and farthest from (Column 1 or 46) the nadir track, respectively. Figure 5 indicates that the difference in the wind speed retrieval errors between these two algorithms is not very significant, in spite of a slight improvement being made by the modified algorithm.

**Table 2.** Wind retrieval errors for the different regions of the swath

| Error | Region | Traditional algorithm | Advanced algorithm |
|---|---|---|---|
| Wind speed MAE/ m·s$^{-1}$ | nadir | 0.12 | 0.12 |
| | middle | 0.07 | 0.07 |
| | outer | 0.23 | 0.22 |
| Wind speed RMSE/ m·s$^{-1}$ | nadir | 0.18 | 0.17 |
| | middle | 0.10 | 0.10 |
| | outer | 0.75 | 0.61 |
| Wind direction MAE/(°) | nadir | 4.04 | 3.35 |
| | middle | 2.87 | 2.72 |
| | outer | 7.84 | 6.16 |
| Wind direction RMSE/(°) | nadir | 10.38 | 9.79 |
| | middle | 9.24 | 8.54 |
| | outer | 18.43 | 16.40 |

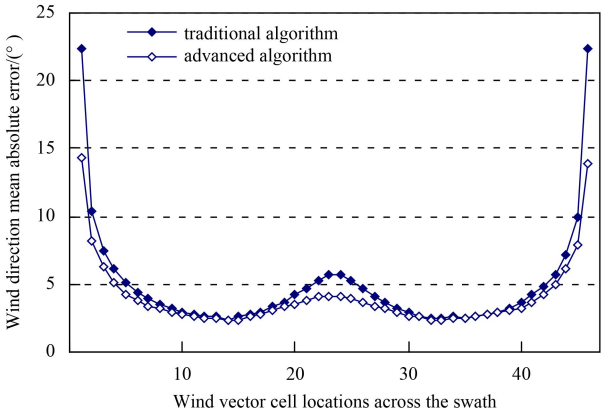


**Fig. 5.** Variations of wind direction mean absolute error versus wind vector cell location for the modified and traditional algorithms.

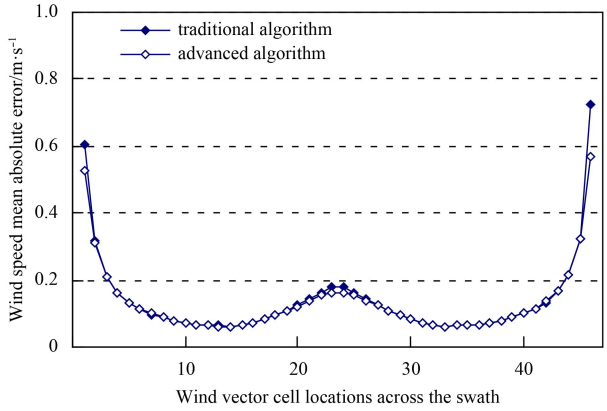


**Fig. 6.** Variations of wind speed mean absolute error versus wind vector cell location for the modified and traditional algorithms.

All the statistical results in Table 2, Figs 5 and 6 were calculated by comparing the retrieved wind vectors with the input reference wind fields. In Table 2, we divided the whole data set into three groups, according to the three regions of the swath, and computed the statistical parameters for each region. Thus, the wind vector errors in Table 2 are actually the average levels for the corresponding swath region, whereas, in Figs 5 and 6, the errors are computed on the basis of each wind vector cell column, representing the average level of the wind vector cells belonging to that column. Hence, Figs 5 and 6 reflect the variations of the wind retrieval errors with the wind vector cell position across the swath.

Figures 7 and 8, respectively, present the portions of the wind fields for orbit 10165 retrieved by the traditional MLE algorithm and the advanced algorithm. For comparison, the corresponding portion of the input wind field is given in Fig. 9. The rows of the wind field shown in the figures are from 1 080 to 1 140. Figure 7 shows that some of the wind directions located in the red rectangular box (left area of the wind field) clearly exhibit inconsistencies. In contrast, a more continuous and coherent wind field is obtained by the new integrated algorithm in the same region, as displayed in Fig. 8. In comparison with Fig. 9, the wind field retrieved by the integrated algorithm is much closer to the input wind field.

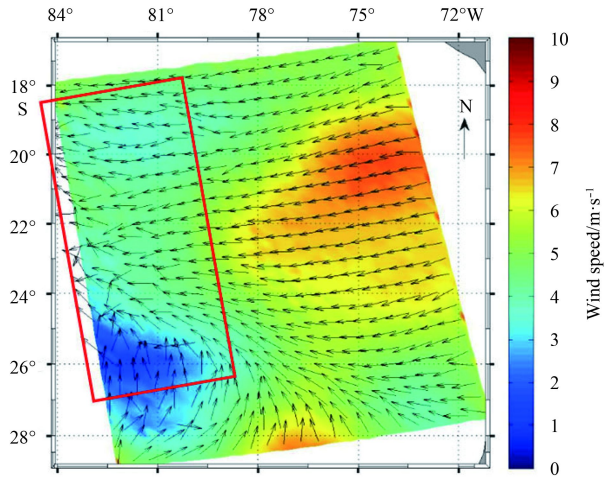


**Fig. 7.** The wind field retrieved by the traditional MLE algorithm.

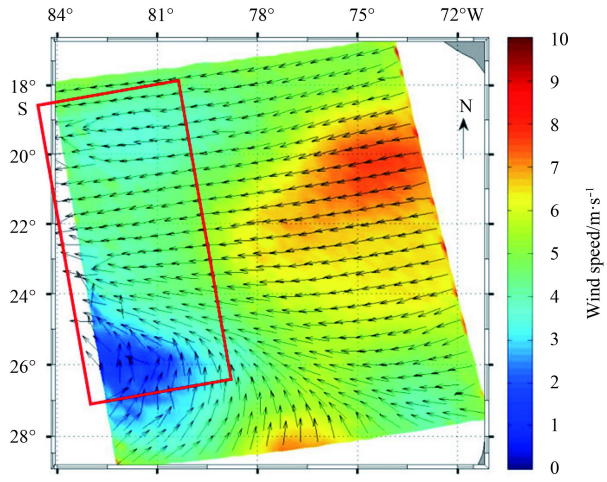


**Fig. 8.** The wind field retrieved by the advanced algorithm.

## 5 Conclusions

Owing to the main shortcomings of the conventional MLE algorithm, an advanced wind vector retrieval algorithm for the RFSCAT has been developed based on its particular observation geometry. The proposed algorithm can improve the wind direc-

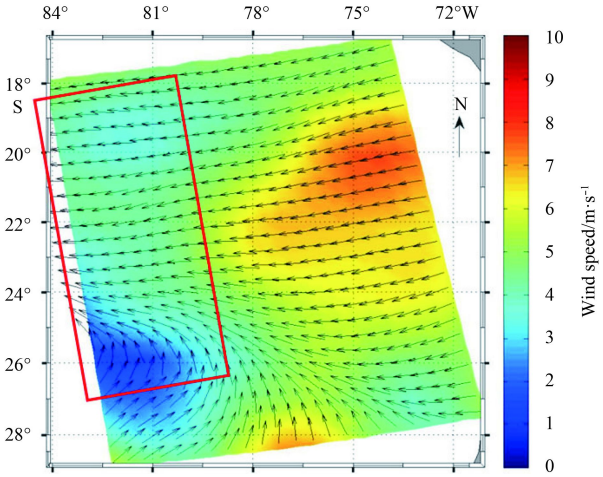


**Fig. 9.** The input reference wind field.

tion retrieval accuracy for most wind vector cell positions across the whole swath, especially in the nadir and outer regions. This advantage comes from the capability to adaptively extend the ambiguity wind directions depending on the wind retrieval errors under the condition of the traditional MLE.

It should be noted that the rate threshold values are extremely crucial in the new algorithm. Only a preliminary validation was conducted in this paper. Careful tuning should be done to optimize the threshold values of the wind speed standard deviation in order to further improve the wind retrieval accuracy.

***Acknowledgements***

The authors thank PO.DAAC for providing the SeaWinds L2B data.

**References**

Arnús M P. 2002. Wind field retrieval from satellite radar systems [dissertation]. Barcelona: University of Barcelona

Chi C Y, Li F K. 1988. A comparative study of several wind estimation algorithms for spaceborne scatterometers. IEEE Transactions on Geoscience and Remote Sensing, 26(2): 115–121

Dunbar R S. 2006. Level 2B data software interface specification (SIS-2): QuikSCAT Era. ftp://www.scp.byu.edu/data/qscat/docs/L2B_SIS_200609.pdf [2006-09-27/2013-05-15]

Fischer R. 1972. Standard deviation of scatterometer measurements from space. IEEE Transactions on Geoscience Electronics, 10(2): 106–113

Freilich M H. 2000. SeaWinds algorithm theoretical basis document. http://eospso.nasa.gov/sites/default/files/atbd/atbd-sws-01.pdf [1996-07-19/2002-09-11]

JPL. 2003. SeaWinds on ADEOS-II Level 2B ocean wind vectors in 25 km swath. Version 1. 2. Provo: Brigham Young University, http://www.scp.byu.edu/pub/docs/ProjDocs/SWS_L2B.pdf [2003-10-14/2016-08-13]

Lin C C, Stoffelen A, de Kloe J, et al. 2003. Wind retrieval capability of rotating, range-gated, fanbeam spacborne scatterometer. In: Proceedings of SPIE- Sensors, Systems, and Next-Generation Satellites. Washington: Bellingham, 4881: 268–279

Long D G, Chi C Y, Li F. 1988. The design of an onboard digital Doppler processor for a spaceborne scatterometer. IEEE Transactions on Geoscience and Remote Sensing, 26(6): 869–878

Lungu T. 2001. QuikSCAT science data product user's manual. Version 2.2. Provo: Brigham Young University, ftp://www.scp.byu.edu/pub/docs/ProjDocs/QSUG4-4.pdf [2005-12-09/2010-08-26]

Shaffer S J, Dunbar R S, Hsiao S V, et al. 1991. A median-filter-based ambiguity removal algorithm for NSCAT. IEEE Transactions on Geoscience and Remote Sensing, 29(1): 167–174

Stiles B W, Pollard B D, Dunbar R S. 2002. Direction interval retrieval with thresholded nudging: a method for improving the accuracy of QuikSCAT winds. IEEE Transactions on Geoscience and Remote Sensing, 40(1): 79–89

Ulaby F T, Moore R K, Fung A K. 1986. Microwave Remote Sensing: Active and Passive, Vol. 3. Norwood: Artech House, 1065–2162

Wang Zhixiong, Zhao Chaofang, Zou Juhong, et al. 2015. An improved wind retrieval algorithm for the HY-2A scatterometer. Chinese Journal of Oceanology and Limnology, 33(5): 1201–1209

Kloe J, Stoffelen A. 2003. Optimisation of rotating, range-gated fanbeam scatterometer for wind retrieval. Task 3a Report: Fom Definition and Validation. Amsterdam: Royal Netherlands Meteorological Institute. http://projects.knmi.nl/publications/fulltexts/rfscat_task_3a_report.pdf [2003-04-03/2008-12-25]

Xie Xuetong, Huang Zhou, Lin Mingsen, et al. 2013. A novel integrated algorithm for wind vector retrieval from conically scanning scatterometers. Remote Sensing, 5(12): 6180–6197

Xie Xuetong, Lin Mingsen, Huang Zhou, et al. 2010. A modified wind vector retrieval algorithm for polarimetric scatterometer. In: Proceedings of 2010 IEEE International Geoscience and Remote Sensing Symposium. Honolulu: Curran Associates, 4184–4187